Early snowmelt significantly enhances boreal springtime carbon uptake

Jouni Pulliainen[a,1], Mika Aurela[a], Tuomas Laurila[a], Tuula Aalto[a], Matias Takala[a], Miia Salminen[a], Markku Kulmala[b], Alan Barr[c,d], Martin Heimann[e,f], Anders Lindroth[g], Ari Laaksonen[a], Chris Derksen[c], Annikki Mäkelä[h], Tiina Markkanen[a], Juha Lemmetyinen[a], Jouni Susiluoto[a], Sigrid Dengel[i], Ivan Mammarella[j], Juha-Pekka Tuovinen[a], and Timo Vesala[f,h,j]

[a]Finnish Meteorological Institute, FIN-00101 Helsinki, Finland; [b]Department of Physics, University of Helsinki, FI-00014 Helsinki, Finland; [c]Climate Research Division, Environment and Climate Change Canada, Toronto, ON M3H 5T4, Canada; [d]Global Institute for Water Security, University of Saskatchewan, Saskatoon, SK S7N 3H5, Canada; [e]Max Planck Institute for Biogeochemistry, 07701 Jena, Germany; [f]Department of Physics, University of Helsinki, FI-00014 Helsinki, Finland; [g]Department of Physical Geography and Ecosystems Science, Lund University, SE-22362 Lund, Sweden; [h]Department of Forest Sciences, University of Helsinki, FI-00014 Helsinki, Finland; [i]Climate & Ecosystem Sciences Division, Lawrence Berkeley National Laboratory, Berkeley, CA 94721; and [j]Viikki Plant Science Centre, University of Helsinki, FI-00014 Helsinki, Finland

Edited by F. Stuart Chapin III, University of Alaska, Fairbanks, AK, and approved September 5, 2017 (received for review May 11, 2017)

We determine the annual timing of spring recovery from space-borne microwave radiometer observations across northern hemisphere boreal evergreen forests for 1979–2014. We find a trend of advanced spring recovery of carbon uptake for this period, with a total average shift of 8.1 d (2.3 d/decade). We use this trend to estimate the corresponding changes in gross primary production (GPP) by applying in situ carbon flux observations. Micrometeorological CO_2 measurements at four sites in northern Europe and North America indicate that such an advance in spring recovery would have increased the January–June GPP sum by 29 g·C·m^{-2} [8.4 g·C·m^{-2} (3.7%)/decade]. We find this sensitivity of the measured springtime GPP to the spring recovery to be in accordance with the corresponding sensitivity derived from simulations with a land ecosystem model coupled to a global circulation model. The model-predicted increase in springtime cumulative GPP was 0.035 Pg/decade [15.5 g·C·m^{-2} (6.8%)/decade] for Eurasian forests and 0.017 Pg/decade for forests in North America [9.8 g·C·m^{-2} (4.4%)/decade]. This change in the springtime sum of GPP related to the timing of spring snowmelt is quantified here for boreal evergreen forests.

carbon uptake | earth observation | snowmelt

High-latitude warming and an associated reduction in spring snow cover are expected to have complex impacts on regional climate patterns and ecological responses (1, 2). The timing of spring recovery of photosynthesis in boreal evergreen forest following snowmelt is one of the major factors affecting the carbon balance across high latitudes (3–5). The integrated effect of anthropogenic impacts on climate causes the total radiative forcing to be positive, which increases the heat balance of the atmosphere. The largest individual cause of warming is the anthropogenic increase in CO_2 concentration (6), which is controlled by the response of the global carbon cycle to anthropogenic CO_2 emissions. Recent studies have documented, with very high confidence, that the world's forests constitute an important carbon sink (4, 6, 7). The annual total boreal forest net carbon sink is estimated to be 0.5 ± 0.1 Pg·C·y^{-1} for the 2000–2007 period (4). Based on coupled carbon cycle–climate modeling, this sink is estimated to be increasing by 0.014 Pg·C·y^{-1} for boreal North America including all land areas and by 0.018 Pg·C·y^{-1} for boreal Asia, respectively (7). However, considerable uncertainty remains regarding the magnitude of this terrestrial sink, particularly how it changes with time due to external climate drivers including the timing of spring snowmelt. It is vital for future climate scenarios to reduce the forest sink uncertainty and obtain information on the spatiotemporal variability and trends. High-latitude warming over the land surface is associated with observed reductions in spring snow extent through earlier snowmelt (2, 8–10). Advanced snowmelt across the boreal zone has a potentially major impact on the carbon balance (11–14). Here, we combine spatially continuous time series of satellite-derived snowmelt data (clearance from the landscape, that is, the time when fractional snow cover reaches zero) with point-wise carbon flux observations to address this open question. This is performed by quantifying the relationship between the observed declines in spring snow cover extent (due to earlier snowmelt) and the carbon balance in springtime.

Results

We define the dynamics of boreal forest carbon uptake by using the change of snow clearance day (SCD) as a proxy indicator for changes in evergreen boreal forest spring recovery (SR) of photosynthesis, defined here as the timing in spring when the ecosystem CO_2 uptake exceeds 15% of its summertime maximum. Timing of SR is a major factor influencing the springtime carbon balance of high-latitude boreal forests (15–17). The advance of SR is associated with an increase in the spring carbon sink that can be quantified in terms of net ecosystem production (NEP) or gross primary production (GPP). CO_2 flux-derived NEP and GPP time series obtained for a Canadian Jack Pine forest demonstrate the connection between the advance of SR and the increase in carbon uptake (Fig. 1). Note that NEP is equivalent to GPP minus ecosystem respiration. We develop a unique approach for monitoring SR over the Earth's boreal forest zone by exploiting recent Earth Observation (EO) time series. We compare hemispheric long-term

Significance

We quantified a 36-y trend of advanced spring recovery of carbon uptake across the northern hemisphere boreal evergreen forest zone. From this trend, we estimated the corresponding change in global gross primary production (GPP) and further quantified the magnitude and spatiotemporal variability of spring GPP, that is, the cross-photosynthetic carbon uptake by forest. Our main findings are the following: (*i*) We developed a proxy indicator for spring recovery from in situ flux data on CO_2 exchange and recent satellite snowmelt products and (*ii*) we established a relation between spring recovery and carbon uptake to assess changes in springtime carbon exchange showing a major advance in the CO_2 sink.

Author contributions: J.P., M.A., T.A., and T.V. designed research; J.P., M.A., T.A., C.D., A.M., T.M., and J.S. performed research; M.T. and J.L. contributed new analyses tools; J.P., M.A., T.L., T.A., M.S., T.M., J.S., S.D., I.M., and J.-P.T. analyzed data; J.P., M.A., T.A., M.S., M.K., A.B., M.H., A. Lindroth, A. Laaksonen, C.D., A.M., T.M., and T.V. wrote the paper; and A.B., M.H., A. Lindroth, S.D., and I.M. provided flux data.

The authors declare no conflict of interest.

This article is a PNAS Direct Submission.

Freely available online through the PNAS open access option.

[1]To whom correspondence should be addressed. Email: jouni.pulliainen@fmi.fi.

This article contains supporting information online at www.pnas.org/lookup/suppl/doi:10.1073/pnas.1707889114/-/DCSupplemental.

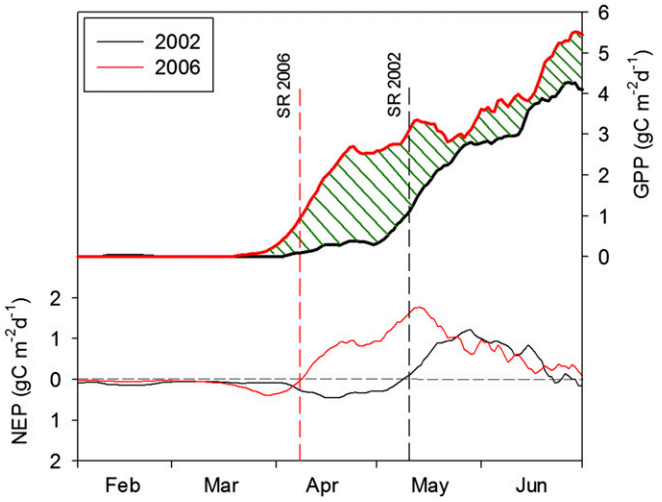

Fig. 1. Relation between SR date and carbon uptake of boreal forests in terms of GPP (thick lines, *Upper*) and NEP (thin lines, *Lower*). Daily (15-d running mean) GPP and NEP during two contrasting springs at an old-growth Jack Pine forest site in Canada demonstrate the effect of the advanced SR on the carbon uptake for a single site. Vertical dashed lines depict the flux-data–derived estimate of SR while green shading illustrates the increase in GPP during earlier spring (shaded area corresponding to change in carbon sink/uptake).

passive microwave satellite retrievals of SCD with in situ SR estimates from CO_2 flux-tower measurements. The method facilitates the use of SCD as an indicator for evergreen boreal forest spring recovery. This is necessary because no method has yet been developed to directly retrieve the recovery of photosynthesis or carbon uptake by forests from satellite observations for long periods across the northern hemisphere boreal zone. Annual spring recovery maps are generated for the 36-y microwave satellite data record. The uniqueness of this time series is its temporal precision achieved through complete passive microwave satellite coverage of boreal and high-latitude land areas every 1–2 d.

SCD information is derived solely from analysis of the space-borne passive microwave radiometer time series (10) (Fig. 2), which provides continuous coverage regardless of cloud and illumination conditions. Through the comparison of satellite retrievals with in situ data (SR derived from eddy covariance tower measurements of CO_2 fluxes in Finland, Sweden, Canada, and Russia), a linear regression model is established to describe SR as a function of SCD (Fig. 3). Based on the regression formula, the spatial patterns of SR can be mapped (Fig. 2) and temporal variability and trends in SR determined (Figs. 2 and 4 and Table 1). For comparison, SR is also analyzed using an independent landscape freeze/thaw Earth system data record (FT-ESDR) also determined from space-borne microwave radiometer data (18). Our SCD estimates and the FT-ESDR spring thaw estimates are highly correlated despite different retrieval approaches. We place added confidence in our approach because comparison with SCD derived from weather station observations indicates that the SCD dataset has a higher correlation with observed snowmelt than FT-ESDR. Note that FT-ESDR is highly correlated with the near-surface air temperature, as reanalysis-based air temperature is used for calibration of freeze/thaw retrievals (18).

We estimated the in situ SR through CO_2 net ecosystem exchange (NEE, equivalent to –NEP) measured at eddy covariance flux towers; see *Materials and Methods* for details. The 10 stations employed for regression analysis are located in Finland (4), Sweden (2), Canada (2), and Russia (2), representing conifer-dominated northern, central, and southern boreal forests. Flux observations from the stations cover different time periods between 1996 and 2014 and collectively provide 84 SR dates. The comparison of satellite data with in situ SR (Fig. 3) shows that SCD retrievals can be used as a proxy indicator for the spatial patterns of SR for coniferous forests. The coefficient of determination (R^2) of the

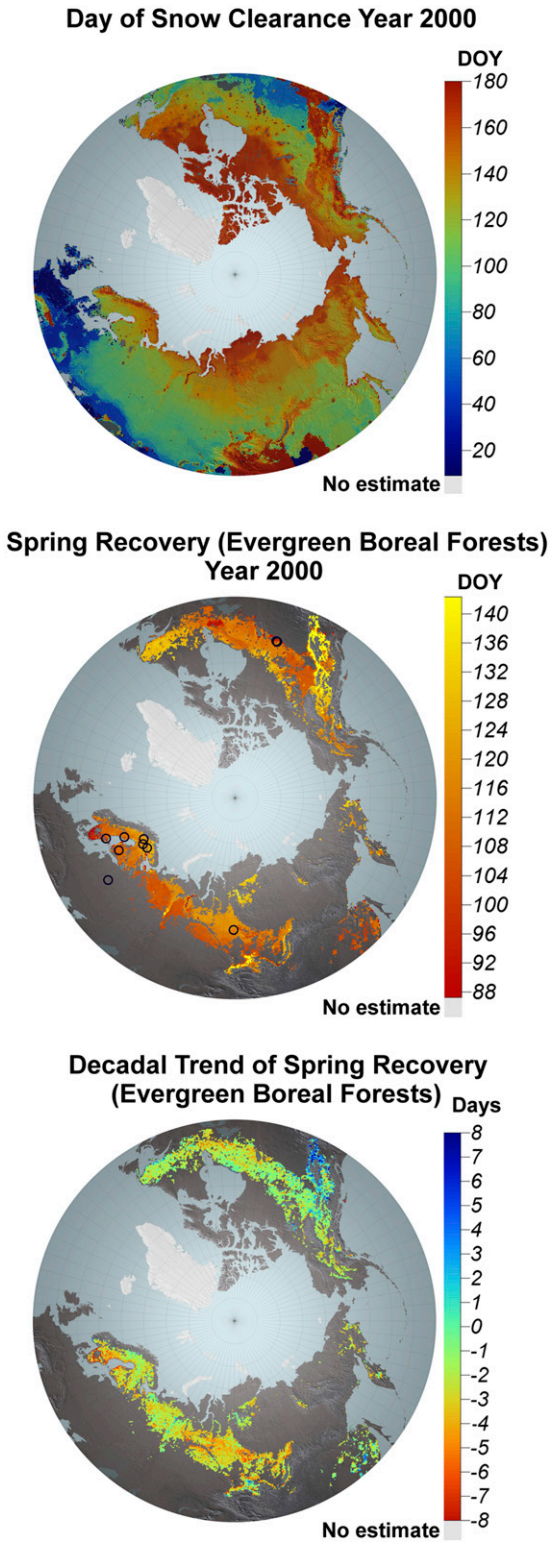

Fig. 2. SCD used as a proxy indicator for SR. (*Top*) SCD for the year 2000, retrieved from space-borne microwave radiometry. (*Middle*) The spatial behavior of SR for the year 2000 [day of year (DOY) for SR based on Eq. **1**]. CO_2 flux measurement stations (10) are depicted by circles. (*Bottom*) Estimated decadal trend (days per decade) of SR determined over the period 1979–2014.

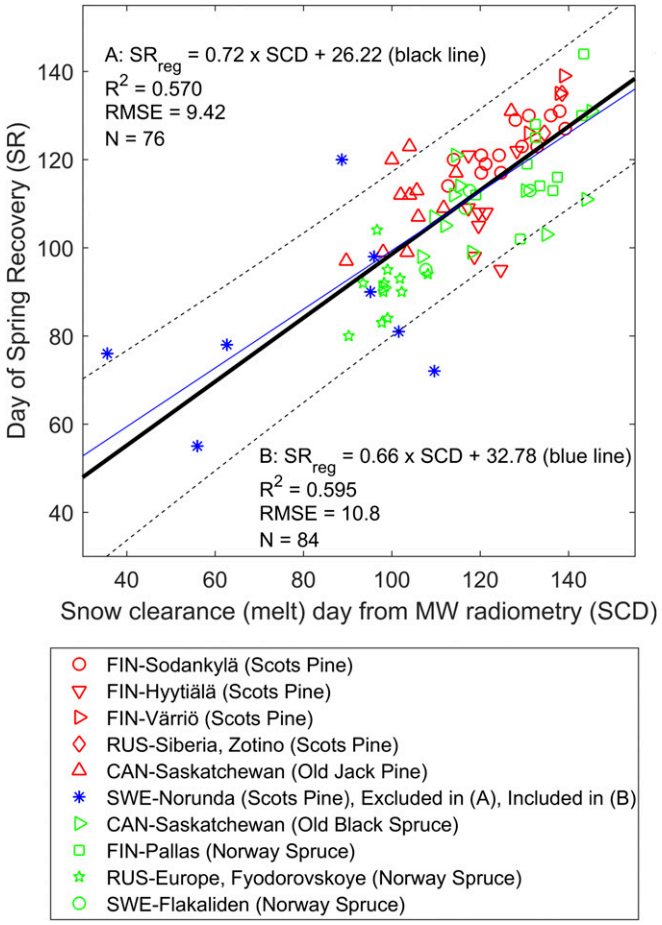

Fig. 3. Proxy for SR. Relation between CO_2 flux-tower data-derived SR and SCD from microwave radiometry for 10 conifer-dominated sites representing southern, central, and northern boreal forests. The flux stations include treated forests (harvested in the past) as well as natural forests (including forests with uniform age structure suggesting regeneration following wildfire). The regression equation between SCD and SR, used as a proxy indicator for SR, is also shown: The line of regression is shown by a black line and the 95% prediction band of the regression equation by dashed lines (case A), whereas the regression including Norunda data from the ephemeral snow region is depicted by a blue line (case B).

linear regression was 0.57 and the root mean-square error (statistical accuracy) was 9.4 d. FT-ESDR data on landscape freeze/thaw state were employed similarly to establish the regression relation between SR and the landscape thaw estimate. A slightly lower coefficient of determination was obtained ($R^2 = 0.52$). Table 1 shows the decadal change of SR for evergreen boreal forests obtained using both SCD and FT-ESDR as proxies. Both data sources provide SR estimates and trends that agree with each other within statistical error margins.

SCD can be used as a proxy for SR because of the tight coupling between snowmelt, soil thaw, and the onset of transpiration and photosynthesis (17, 19, 20). While soil thaw can be a critical factor affecting SR via the availability of water to roots, earlier work has demonstrated that photosynthesis can begin across a range of soil temperatures, following the rise of near-surface air temperature through a dynamic delay response (13, 16, 19). In regions with seasonal snow cover, the onset of snowmelt immediately precedes soil thaw that starts from the top of and bottom of the frozen layer (21, 22). The soil begins to thaw well before snow clearance is completed, triggered by the infiltration of water from the melting snowpack. Snow melt and clearance are also related to daily air temperature and are often described in hydrology with a simple degree day model (21), similar to the dynamic delay response of photosynthesis (23). Thus, our basic

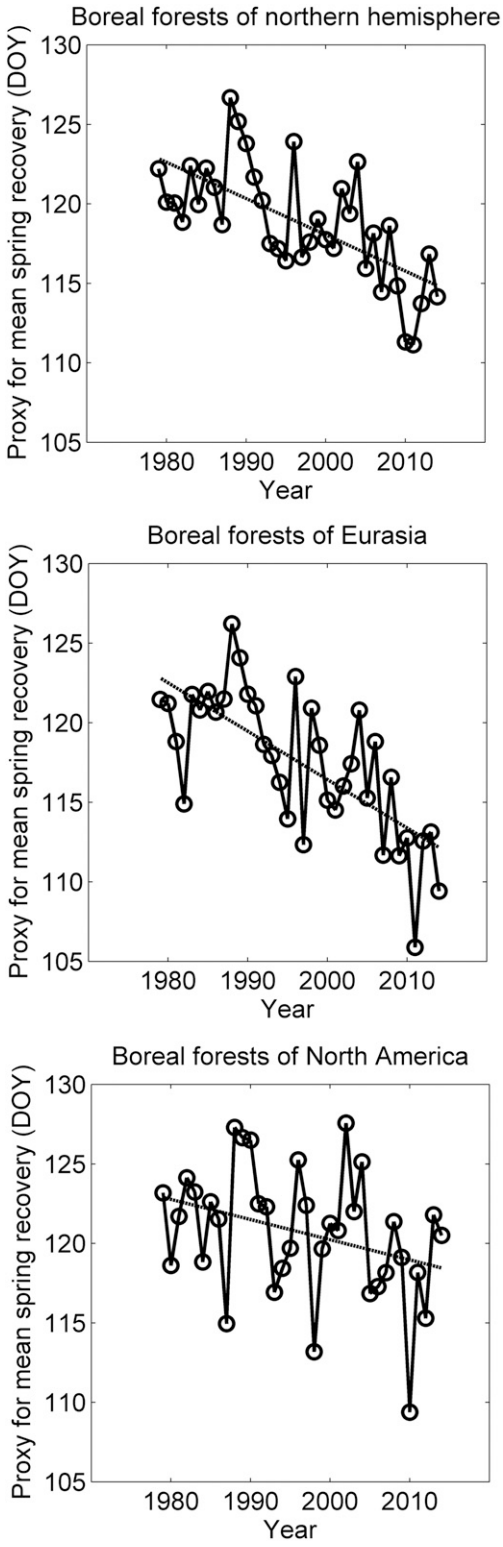

Fig. 4. SR trends in northern hemisphere. Estimated yearly time series of mean SR are shown for conifer boreal forests of northern hemisphere, Eurasia, and North America based on the regression equation of Fig. 3. Trend lines by linear regression are also shown (see Table 1 for numerical results).

Table 1. The extent of the evergreen boreal forest used in the spring recovery (SR) analysis, the change of SR based on trend lines estimated by linear regression (± intervals based on 95% confidence bounds from Eq. 1), *P* values of trend lines, and the corresponding decadal change of carbon sink (GPP)

Region	Forested area, 10^6 km^2	ΔSR, change of spring recovery,* d/decade	*P* value for SR trend line	ΔGPP_{spring}, increase of springtime GPP†	
				Pg C/decade	g·C·m^{-2}/decade
Northern hemisphere	3.95	−2.28 ± 0.46 (−1.99 ± 0.46)	$1.0 \cdot 10^{-5}$	0.052† (5.8%) 0.033 ± 0.004‡	13.1† 8.4 ± 1.7‡
Eurasia	2.26	−3.04 ± 0.61 (−2.40 ± 0.55)	$1.4 \cdot 10^{-6}$	0.035† (6.8%) 0.022 ± 0.005‡	15.5† 9.9 ± 2.0‡
North America	1.69	−1.27 ± 0.25 (−1.44 ± 0.33)	0.05	0.017† (4.4%) 0.009 ± 0.002‡	9.8† 5.2 ± 1.0‡

In parentheses is the change of SR estimated from the FT-ESDR dataset, using the same regression method.
*ΔSR estimated from the satellite observations.
†Global model-simulated ΔGPP_{spring} (6-mo sum of daily GPP).
‡Increase of GPP estimated using ΔSR values of the three regions and average $\delta GPP_{spring}/\delta SR$ values determined for (*i*) two flux stations in Eurasia, (*ii*) two stations in North America, and (*iii*) all four stations in the hemispheric case: $\Delta GPP_{spring} = \Delta SR \times \delta GPP_{spring}/\delta SR$.

assumption that the SCD derived from microwave data may be used as a proxy for boreal forest SR has a strong biophysical justification.

Our results indicate a trend toward earlier snow clearance from the landscape, with a related shift to earlier SR (Fig. 4 and Table 1). This hemispheric trend is driven almost entirely by Eurasia, where the start of the growing season is ∼11 d earlier by the end of the time series (1979–2014). For North America the change is smaller and the interannual variability is larger. The influence of advanced SR on springtime carbon uptake was quantified by analyzing the flux measurement-based 6-mo GPP sum starting from the beginning of the year (GPP_{spring}) at four sites having a sufficient number of observation years; two forests in northern Finland [Kenttärova (N67.98, E24.25) and Sodankylä (N67.37, E26.63) sites] and two forests in Canada [old Jack Pine (OJP) (N53.92, W104.69) and old Black Spruce (OBS) (N53.99, W105.12) sites]. When combined with the hemispheric advance of SR, the average observed sensitivity of GPP_{spring} to satellite-derived SR ($\delta GPP_{spring}/\delta SR$) suggests an increase of 8.4 g·C·m^{-2} (3.7%)/decade in GPP_{spring} for such boreal forests (Table 1).

Additionally, global climate model simulations provided the change of GPP_{spring} for all of the model grid cells covered by boreal forest. These estimates confirm that the earlier SR affects the decadal carbon sink (uptake) during spring within the whole region (Table 1). It is well known that the representation of vegetation phenology could be improved in many ecosystem models (24). However, testing a different temperature response for GPP in our model retained the sensitivity of GPP to SR, confirming that the result is robust. The correlation between early onset of SR and the level of midsummer GPP was also investigated by comparing satellite data retrievals of SR with the model-predicted July–August GPP sum. The analysis was carried out for all pixels representing evergreen boreal forests (over 11,000 pixels with a size of 625 km^2). The results show a weak positive correlation between the early onset of uptake and the higher level of GPP during the midsummer, even though a small negative correlation was found for some regions (Fig. S1).

We investigated the validity of the modeling approach by comparing the modeled springtime GPP sums with satellite-derived SR (sensitivity $\delta GPP_{spring}/\delta SR$) through Eurasia and North America and by comparing $\delta GPP_{spring}/\delta SR$ values with those observed for Canadian and Finnish flux sites (Fig. 5). Flux data analysis provided $\delta GPP_{spring}/\delta SR$ values ranging from −3.0 to −4.1 g·C·m^{-2}·d^{-1}. The sensitivities obtained from the model predictions showed a mean value of −2.2 g·C·m^{-2}·d^{-1} with a SD of 1.4 g·C·m^{-2}·d^{-1} for Eurasian forests and mean of −2.3 g·C·m^{-2}·d^{-1} with a SD of 1.6 g·C·m^{-2}·d^{-1} for North American forests, respectively (Fig. 6). This indicates that the applied flux stations represent typical boreal forest in terms of $\delta GPP_{spring}/\delta SR$.

Earlier work applying satellite data for boreal forests has primarily used channel fraction indexes such as normalized difference water index (NDWI) and normalized difference vegetation index (NDVI), determined from optical satellite data (25, 26) to investigate the start of the growing season in relation to phenological observations (e.g., timing of bud burst) or modeled phenological indexes (26, 27). Especially in the case of evergreen coniferous forests, only a small number of investigations have directly used CO_2 flux measurements as reference (28, 29). A previous case study on conifer-dominated boreal forests in Finland showed that snowmelt information derived from optical satellite data provides better estimates of SR than the normalized difference snow index (NDSI) or NDWI (29).

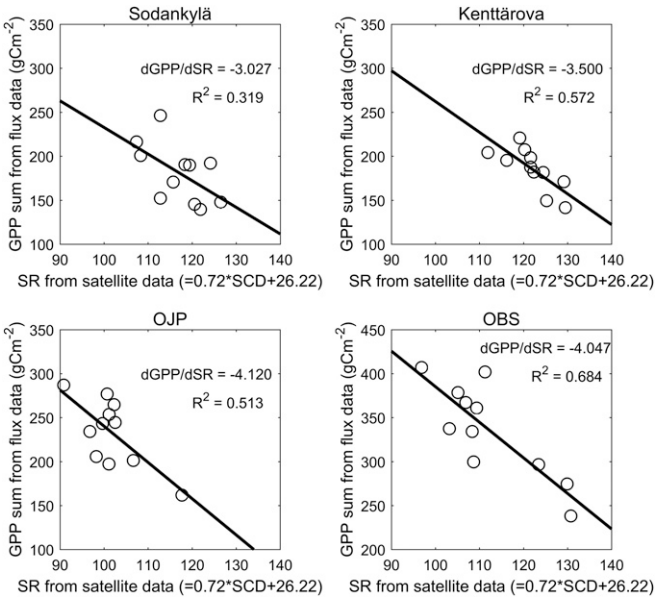

Fig. 5. Relation between satellite data (microwave radiometry)-derived SR date and carbon uptake (6-mo GPP sum, January–June) determined from CO_2 observations at flux towers. Four sites in Canada and Finland provided 11 annual observations of GPP_{spring}, enabling the estimation of sensitivity $\delta GPP_{spring}/\delta SR$ through linear regression.

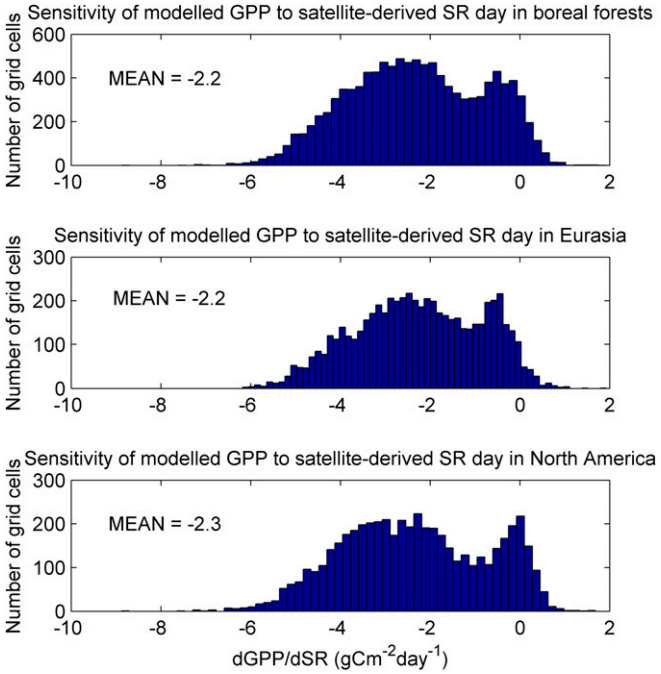

Fig. 6. Sensitivity of modeled GPP_{spring} to satellite data-derived SR for different regions. The sensitivity values are obtained by linear least-squares fitting of SR data to modeled annual springtime GPP sums (January–June) for each grid cell for 1979–2014. The slope of the regression line provides the sensitivity $\delta GPP_{spring}/\delta SR$.

Although our regression results indicate some systematic differences between the flux stations, the overall relationship between SR and SCD is strong (Fig. 3). There is no indication that the differences among stations arise from differences in tree species or region, that is, southern, central, or northern boreal forest. The SR of photosynthesis has also been found to follow environmental drivers according to a general pattern across different types of boreal coniferous forest (30). An obvious constraint of the methodology is the requirement of the presence of persistent seasonal snow cover, as demonstrated by the results for Norunda, Sweden. The Norunda data show more scatter (Fig. 3) because of its ephemeral (transitory) snow conditions. Fortunately, the proportion of boreal forest with ephemeral snow is very small. Another factor that weakens the correlation between SR and SCD is a large difference in the size of their respective footprints: ~25 km spatial resolution for SCD from space-borne microwave radiometer data, compared with a few hundred hectares for eddy-covariance measurements above forests.

Discussion

Our results show that passive microwave satellite-derived estimates of SCD can be combined with continuous CO_2 flux measurements to retrieve the trends of boreal forest SR (Fig. 3). The trend over 36 y is statistically significant for both Eurasia and North America and particularly strong for Eurasia (Table 1). This trend results in a significant increase in the springtime carbon uptake for Eurasia over the investigated period (Table 1). Here we affirm the important role of EO in producing spatial and temporal information on variability in the carbon cycle not available from flux-tower measurements alone. Thus, combining EO and in situ flux data is a powerful tool to move from direct geophysical retrievals (snow clearance) to high-order parameters (SR and carbon uptake). The numbers obtained here for the advancement of SR (0.23 d/y for the whole region) are consistent with the observed longer-term advance of the seasonal cycle of atmospheric CO_2 in high latitudes, such as 0.17 d/y measured at Barrow, AK (31). An increase in the equivalent photosynthetic active period of 0.48 d/y has been estimated for the boreal zone (figure 3d in ref. 32). This estimate is for the entire year, but it is consistent with our estimates, which are for springtime (6 mo) only. Our estimates of increasing GPP in spring for the boreal forest are comparable to model predictions of annual net primary production reported elsewhere (7). This is apparent since our results suggest that there is typically a slight positive correlation between the early onset of carbon uptake and the level of July–August GPP.

The recent boreal warming trend causes earlier SR, which increases the carbon uptake during spring. This negative feedback loop reduces radiative forcing, in part counteracting the positive feedback of the earlier snowmelt (shown here) that reduces the albedo. Concerning the annual carbon cycle, earlier studies suggest that the increased soil respiration due to autumn warming may offset 90% of the increased CO_2 uptake during spring (33). The results obtained here on springtime uptake may be used to revise the trends in annual carbon balance of boreal forests.

Materials and Methods

Evergreen boreal forest SR dates from in situ CO_2 flux measurements are compared with microwave satellite retrievals of the SCD across the northern hemisphere boreal forest. The analysis focuses on 10 eddy-covariance flux sites in Eurasia and North America for 1996–2014. SR was determined from flux data based on the night–day difference in NEE. (Note that NEE = –NEP, where NEE is typically used for instantaneous exchange while NEP is used for longer-term balances.) Daily δNEE (= $NEE_{night} - NEE_{day}$) was obtained as a difference of 7-d running mean of nighttime [photosynthetic photon flux density (PPFD) < 20 $\mu mol \cdot m^{-2} \cdot s^{-1}$] NEE and 3-d running mean of daytime [photosynthetic photon flux density (PPFD) > 600 $\mu mol \cdot m^{-2} \cdot s^{-1}$) NEE. The summer maximum daily δNEE (δNEE_{max}) across all measurement years at each site (e.g., 2001–2010 in Sodankylä) was estimated as the 90th percentile of the daily δNEE from the 30-d period with the highest uptake on average. The SR for different years was then defined as the date when daily δNEE first exceeded 15% of site specific δNEE_{max}. The data from all stations were analyzed in the same manner, providing an unbiased dataset.

The obtained linear least-squares model between SR and SCD (Fig. 3) is

$$SR_{reg} = \hat{\beta}_1 \, SCD + \hat{\beta}_0, \qquad [1]$$

where $\hat{\beta}_1 = 0.72 \pm 0.15$ d and $\hat{\beta}_0 = 26.2 \pm 17.4$ d (with 95% CIs). The coefficient of determination for Eq. **1** is 0.57. This equation holds for evergreen conifers in regions of seasonal snow cover. Of the 10 flux-tower sites, only Norunda (Sweden), at the southern border of the boreal forest zone, has ephemeral snow conditions and is thus excluded from the determination of Eq. **1**. Nevertheless, the overall behavior of the Norunda data agrees reasonably well with Eq. **1**, and the regression including Norunda data points does not differ statistically significantly from Eq. **1** and Fig. 3. The method according to Eq. **1** was also applied to FT-ESDR data by replacing SCD with the corresponding FT-ESDR landscape freeze-to-thaw transition date.

Based on long-term hemispheric satellite observations of snow cover, derived from daily passive microwave radiometer observations, we derive spatial maps of SCD for each year (Fig. 2, *Top*). The time series analysis algorithm indicates the timing of snow clearance for all hemispheric grid cells with seasonal snow cover (10). This snowmelt dataset has been also applied to construct the European Space Agency (ESA) GlobSnow daily snow water equivalent (SWE) and SCD climate data record (CDR) extending from 1979 to the present (34, 35). The spatial information on SR is generated by applying Eq. **1** to the SCD retrievals (Fig. 2, *Middle*). The boreal forest extent is extracted using a criterion that each grid cell of size 625 km^2 includes conifer evergreen forests for more than 30% of the total area. The forest mask is determined according to ESA GlobCover and ESA Climate Change Initiative (CCI) land cover information (36), with the latter used only to filter out larch-dominated regions of Siberian forests.

The reliability of trends in Fig. 4 was analyzed by adding a random noise (SD 9.42 d from Fig. 3) to every data-point time series of Fig. 4 (a Monte Carlo simulation). This resulted in a worst-case scenario assuming that the confidence of the regression algorithm of Fig. 3 is limited by the interannual variability (i.e., fluctuations arise from the year-to-year variability in the relation between the SR and SCD). This worst-case scenario suggests that there is a likelihood $P > 0.93$ that the trend is negative for the boreal forests of the northern hemisphere, $P > 0.97$ for Eurasian forests and $P > 0.79$ for North American forests, respectively (Figs. S2 and S3).

Carbon cycle–climate model simulations were carried out using the JSBACH ecosystem model (37, 38) coupled with the ECHAM6 global circulation model (39). The simulations for past decades (1957–2014) were performed with the coupled ECHAM/JSBACH model nudged toward observed climate [ERA40 and ERA Interim data (40, 41)], sea surface temperature, and atmospheric CO_2 concentration data. Springtime GPP was estimated for boreal coniferous evergreen forest in all model grid cells with significant coverage of that plant functional type, using the first 180 d of each year over the period of 1979–2014. The change of GPP for the simulation period was estimated in each grid cell by linear regression.

ACKNOWLEDGMENTS. This work is supported by the Academy of Finland CARBARC (285630); ESA GlobSnow; Academy of Finland Centre of Excellence (118780); Academy Professor projects (1284701 and 1282842); Integrated Carbon Observation System (ICOS) (271878) and ICOS-Finland (281255); ICOS-ERIC (281250); and the Nordic Centres of Excellence, DEFROST and CRAICC. Flux-tower measurements for the Russian sites were obtained as part of the TCOS-Siberia European Union (EU) Project (EU Project NEVK2-2001-00143) and supported by the Max-Planck Institute for Biogeochemistry. M.H. was supported in part by the KrasFlux Russian Science Fund project (Grant 14-24-00113).

1. Flanner MG, Shell KM, Barlage M, Perovich DK, Tschudi MA (2011) Radiative forcing and albedo feedback from the northern hemisphere cryosphere between 1979 and 2008. *Nat Geosci* 4:151–155.
2. Brown RD, Mote PW (2009) The response of northern hemisphere snow cover to a changing climate. *J Clim* 22:2124–2145.
3. Liu Yi Y, et al. (2015) Recent reversal in loss of global terrestrial biomass. *Nat Clim Chang* 5:470–474.
4. Pan Y, et al. (2011) A large and persistent carbon sink in the world's forests. *Science* 333:988–993.
5. Grogan P, Jonasson S (2006) Ecosystem CO2 production during winter in a Swedish subarctic region: The relative importance of climate and vegetation type. *Glob Chang Biol* 12:1479–1495.
6. Ciais P, et al. (2013) *Climate Change 2013: The Physical Science Basis*, eds Stocker TF, et al. (Cambridge Univ Press, Cambridge, UK), pp 465–570.
7. Sitch S, et al. (2015) Recent trends and drivers of regional sources and sinks of carbon dioxide. *Biogeosciences* 12:653–679.
8. Derksen C, Brown R (2012) Spring snow cover extent reductions in the 2008-2012 period exceeding climate model projections. *Geophys Res Lett* 39:L19504.
9. Choi G, Robinson DA, Kang S (2010) Changing northern hemisphere snow seasons. *J Clim* 23:5305–5310.
10. Takala M, Pulliainen J, Metsämäki S, Koskinen J (2009) Detection of snow melt using spaceborne microwave radiometer data in Eurasia from 1979-2007. *IEEE Trans Geosci Remote Sens* 47:2996–3007.
11. Aurela M, Laurila T, Tuovinen J-P (2004) The timing of snow melt controls the annual CO_2 balance in a subarctic fen. *Geophys Res Lett* 31:L16119.
12. Black TA, et al. (2000) Increased carbon sequestration by a boreal deciduous forest in years with a warm spring. *Geophys Res Lett* 27:1271–1274.
13. Tanja S, et al. (2003) Air temperature triggers the recovery of evergreen boreal forest photosynthesis in spring. *Glob Chang Biol* 9:1410–1426.
14. Schwartz MD, Ahas R, Aasa A (2006) Onset of spring starting earlier across the northern hemisphere. *Glob Chang Biol* 12:343–351.
15. Suni T, et al. (2003) Interannual variability and timing of growing-season CO_2 exchange in a boreal forest. *J Geophys Res* 108:4265.
16. Thum T, et al. (2009) Spring initiation and autumn cessation of boreal coniferous forest CO_2 exchange assessed by meteorological and biological variables. *Tellus B Chem Phys Meteorol* 61:701–717.
17. Barr AG, Black TA, McCaughey JH (2009) Climatic and phenological controls of the carbon and energy balances of three contrasting boreal forest ecosystems in western Canada. *Phenology of Ecosystem Processes*, ed Noormets A (Springer, New York), pp 3–34.
18. Kim Y, Kimball JS, McDonald KC, Glassy J (2011) Developing a global data record of daily landscape freeze/thaw status using satellite passive microwave remote sensing. *IEEE Trans Geosci Remote Sens* 49:949–960.
19. Mäkelä A, Hari P, Berninger F, Hänninen H, Nikinmaa E (2004) Acclimation of photosynthetic capacity in Scots pine to the annual cycle of temperature. *Tree Physiol* 24: 369–376.
20. Bergh J, Linder S (1999) Effects of soil warming during spring on photosynthesis recovery in boreal Norway spruce stands. *Glob Chang Biol* 5:245–253.
21. DeWalle R, Rango A (2008) *Principles of Snow Hydrology* (Cambridge Univ Press, Cambridge, UK).
22. Rautiainen K, et al. (2014) Detection of soil freezing from L-band passive microwave observations. *Remote Sens Environ* 147:206–218.
23. Peltoniemi M, et al. (2015) A semi-empirical model of boreal forest gross primary production, evapotranspiration, and soil water—Calibration and sensitivity analysis. *Boreal Environ Res* 20:151–171.
24. Richardson AD, et al. (2012) Terrestrial biosphere models need better representation of vegetation phenology: Results from the North American carbon program site synthesis. *Glob Chang Biol* 18:566–584.
25. Zhang L, Friedl M, Schaaf C, Strahler A (2004) Climate controls on vegetation patterns in northern mid- and high latitudes inferred from MODIS data. *Glob Chang Biol* 10: 1133–1145.
26. Delbart N, Le Toan T, Kergoat L, Fedotova V (2006) Remote sensing of spring phenology in boreal regions: A free of snow-effect method using NOAA-AVHRR and SPOT-VGT data (1982-2004). *Remote Sens Environ* 101:52–62.
27. Jönsson A, Eklundh L, Hellström M, Bärring L, Jönsson P (2010) Annual changes in MODIS vegetation indices of Swedish coniferous forests in relation to snow dynamics and tree phenology. *Remote Sens Environ* 114:2719–2730.
28. Gonsamo A, Chen J, Price D, Kurz W, Wu C (2012) Land surface phenology from optical satellite measurement and CO_2 eddy covariance technique. *J Geophys Res* 117: G03032.
29. Böttcher K, et al. (2014) MODIS time-series-derived indicators for the beginning of the growing season in boreal coniferous forest—A comparison with CO2 flux measurements and phenological observations in Finland. *Remote Sens Environ* 140:625–638.
30. Minunno F, et al. (2016) Calibration and validation of a semi-empirical flux ecosystem model for coniferous forests in the boreal region. *Ecol Modell* 341:37–52.
31. Graven HD, et al. (2013) Enhanced seasonal exchange of CO_2 by northern ecosystems since 1960. *Science* 341:1085–1089.
32. Xu L, et al. (2013) Temperature and vegetation seasonality diminishment over northern lands. *Nat Clim Chang* 3:581–586.
33. Piao S, et al. (2008) Net carbon dioxide losses of northern ecosystems in response to autumn warming. *Nature* 451:49–52.
34. Takala M, et al. (2011) Estimating northern hemisphere snow water equivalent for climate research through assimilation of space-borne radiometer data and ground-based measurements. *Remote Sens Environ* 115:3517–3529.
35. Pulliainen J (2006) Mapping of snow water equivalent and snow depth in boreal and sub-arctic zones by assimilating space-borne microwave radiometer data and ground-based observations. *Remote Sens Environ* 101:257–269.
36. Bontemps S, et al. (2011) GLOBCOVER: Products Description and Validation Report (European Space Agency, ESRIN, Italy), Report 2.2.
37. Raddatz TJ, et al. (2007) Will the tropical land biosphere dominate the climate–carbon cycle feedback during the twenty-first century? *Clim Dyn* 29:565–574.
38. Reick CH, Raddatz T, Brovkin V, Gayler V (2013) Representation of natural and anthropogenic land cover change in MPI-ESM. *J Adv Model Earth Syst* 5:459–482.
39. Stevens B, et al. (2013) Atmospheric component of the MPI-M Earth system model: ECHAM6. *J Adv Model Earth Syst* 5:146–172.
40. Uppala SM, et al. (2005) The ERA40 reanalysis. *Q J R Meteorol Soc* 131:2961–3012.
41. Dee DP, et al. (2011) The ERA-interim reanalysis: Configuration and performance of the data assimilation system. *Q J R Meteorol Soc* 137:553–597.

Supporting Information

Pulliainen et al. 10.1073/pnas.1707889114

We compared the yearly onset of uptake (SR estimated from satellite data) with the modeled midsummer (July–August) GPP (Fig. S1). This was done for all satellite pixels representing boreal forests. Similarly, the midsummer GPP was compared with the 6-mo sum of spring GPP. The obtained histograms of correlation coefficient are shown in Fig. S1. The results indicate that (*i*) typically the earlier onset of uptake coincides with the higher level of midsummer GPP than vice versa (even though the correlations are low) and (*ii*) typically a higher level of GPP during spring coincides with a higher level of midsummer GPP [even though for sum pixels (small) negative correlation coefficients can be observed].

We performed an analysis where random noise was added to SR day estimates shown in Fig. 4 of the main text (Fig. S2). The level of random noise is considered as a worst-case scenario based on Fig. 3. That is, in the worst case the observed rms variability of 9.42 d in Fig. 3 is assumed to result from the interannual variability in the relationship between SCD and SR. Note that the spatial variability that evidently causes part of the spread in Fig. 3 does not affect the trend in Fig. 4 (it affects only the overall level of data points, i.e., bias). Thus, adding a random noise with a SD of 9.42 d yields a pessimistic (worst-case) estimate to the variability of each year's data points in Fig. 4. The results are shown in Fig. S3, also indicating the probability of whether the trend is below zero (earlier SR) for the whole hemispheric forest belt, for Eurasian evergreen boreal forests, and for those of North America. According to simulations we can state that the worst-case scenario suggests that there is a likelihood $P > 0.93$ that the trend is negative for the boreal forests of the northern hemisphere, $P > 0.97$ for Eurasian forests, and $P > 0.79$ for North American forests, respectively.

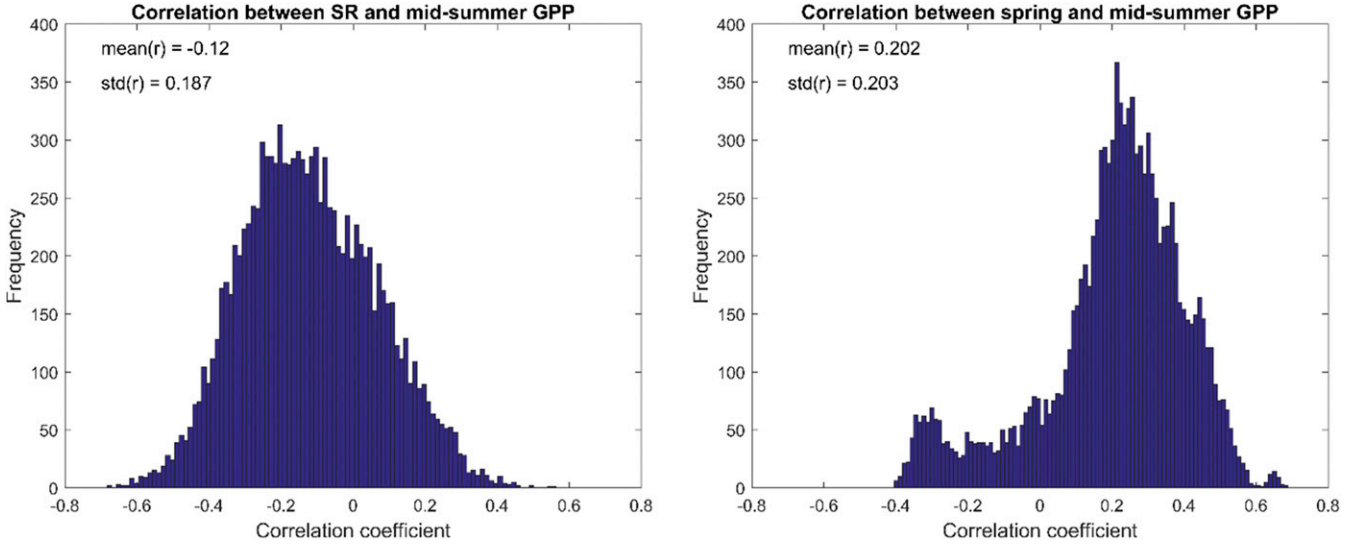

Fig. S1. (*Left*) Correlation between the onset of uptake (SR from satellite data) and July–August GPP. (*Right*) Correlation between January–June GPP and July–August GPP. The histograms are determined for pixel-wise (over 11,000) time series of annual observations and model predictions.

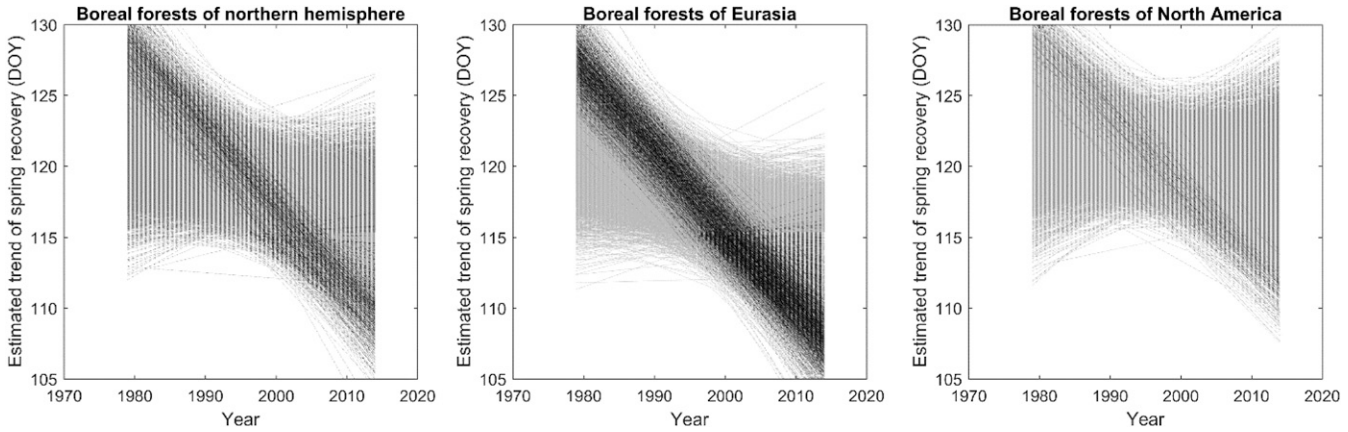

Fig. S2. Trends of spring recovery obtained by a Monte Carlo simulation. Random noise (SD = 9.42 d) is added to time series of Fig. 4: a worst-case scenario assuming that the confidence of the regression algorithm of Fig. 3 is limited by the interannual variability (i.e., fluctuations arise from the year-to-year variability in the relation between the SR and SCD.

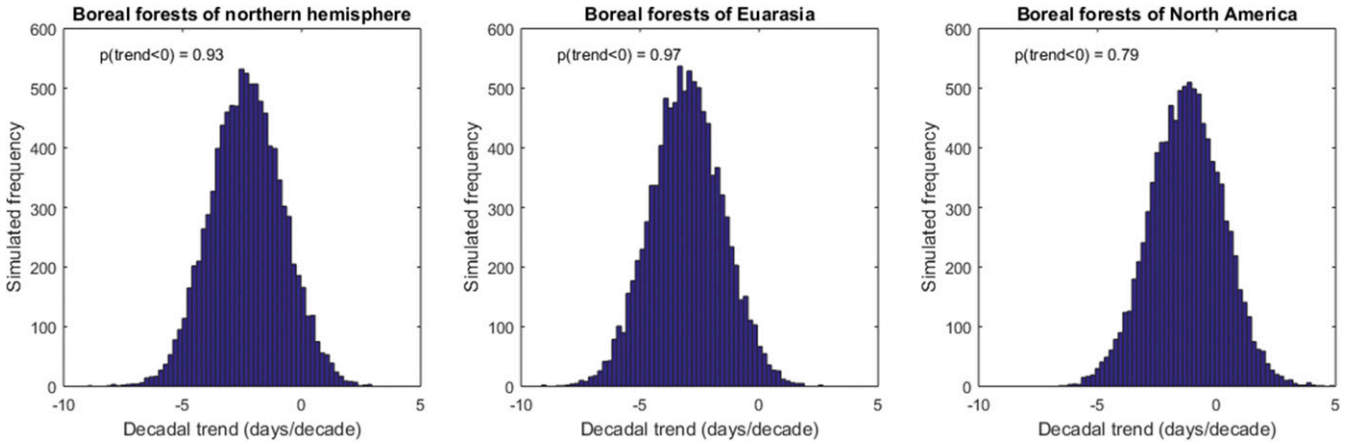

Fig. S3. Histograms corresponding to trends of Fig. S2 with the obtained probabilities that the trend is smaller than zero.